Bad-Honnef Conference on fission and related collective phenomena and properties of heavy nuclei, 1981.

MOMENTUM TRANSFER IN LIGHT ION INDUCED FISSION

F. Saint-Laurent, M. Conjeaud, R. Dayras, S. Harar, H. Oeschler*, C. Volant
DPh-N/BE, CEN Saclay, 91191 Gif-sur-Yvette Cedex, France

presented by S. Harar

I. Introduction

In the fast few years, it has been found experimentally [1] that projectiles up to 35 MeV/A incident energy can transfer their full momentum to heavy nuclei with a significant probability. The aim of the present research was to investigate the momentum imparted to nuclei in an energy range which covers a transition region between compound nucleus formation and cascade nucleon-nucleon interaction of the primary particles and the target nucleus. Experiments were performed at the synchrocyclotron Saturne II of Saclay using proton, deuteron and alpha projectiles from 70 up to 1000 MeV incident energies. The forward component of the linear momentum ($p_{//}$) transferred to the fisionning nuclei was determined by measuring the angle between the resulting fission fragments [2]. The present study was mainly achieved on a ^{232}Th target nucleus because of its high fission cross section which might be closed to the reaction cross sections. In section II, we present briefly the experimental procedure ; in section III the momentum distribution imparted to nuclei is deduced from angular correlation measurements ; in section IV differential and integrated cross sections are presented.

International symposium on nuclear fission and related collective phenomena and properties of heavy ions.
Bad Honnef, RFA, October 26 - 29, 1981.
CEA - CONF 6174

II. Experimental procedure

A residual nucleus which undergoes fission after some initial interaction between projectile and target nucleus, has a momentum which affects the angular correlation between the fission fragments [2]. The longitudinal component of the momentum can be evaluated by measuring fragment-fragment coincidences as a function of the angular position θ_1 and θ_2 of the fragments relative to the beam axis. The first fission detector, fixed at $\theta_1 = -90°$, was perpendicular to the reaction plane, while the second one, covering 8°, was movable and located in the reaction plane on the opposite side of the beam Fig. 1a. Both in-plane and out-plane angular correlations were measured in order to insure that reactions which did not involve formation of a compound nucleus and which possessed momentum components out of the reaction plane were properly taken into account. Detection devices consisted in two identical position-sensitive

*Permanent address : Institut für Kernphysik, D-6100 Darmstadt

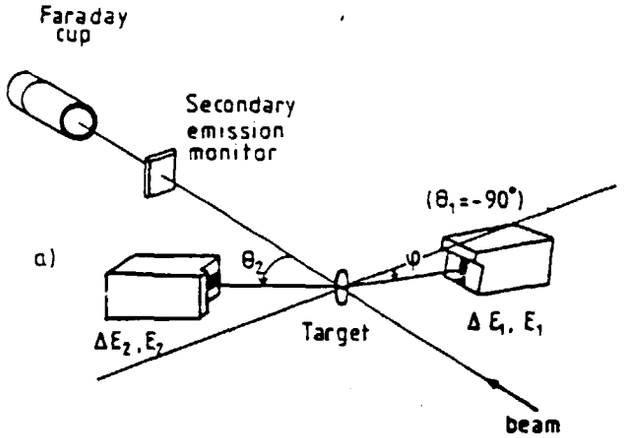

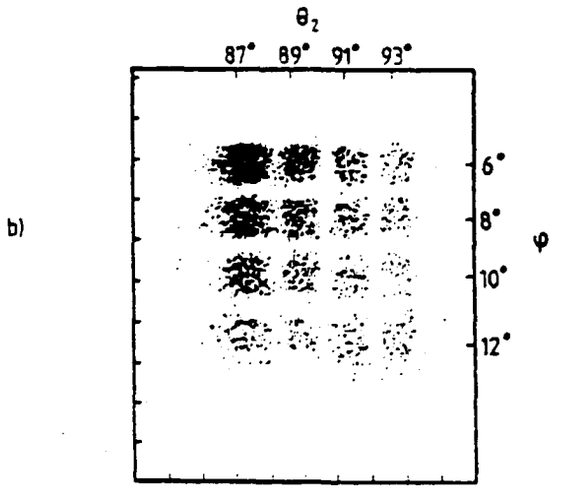

Fig. 1 - a) Experimental set-up. Two identical position sensitive ionization chambers measure the energy losses and total kinetic energies of the fission fragments. Also shown a Faraday cup and a secondary-electron-emission counter to control the beam. b) Each coincidence measurements give simultaneously 16 pairs of angles (in plane θ_2 and out-plane φ).

ionization chambers, operated at 100 torr argon-methane and equipped with a two-stage 12 cm long anode. We measured simultaneously 16 pairs of angles (in and out-plane), Fig. 1b, as well as the fragment fission energies and their losses in the first stage of the detectors. The detectors were calibrated with a ^{252}Cf fission-fragment source.

The target was made by a rolled self-supporting ^{232}Th foil of 1 mg/cm^2 thickness, inclined to 45° relative to the beam axis. The double differential cross sections $d^2\sigma/d\Omega_1 d\Omega_2$ were normalized by using the single yields in the fixed counter (θ_1 = - 90°). A Faraday cup and secondary electron-emission counter served as control and were used for absolute normalization.

At each detection angle, a $E_1 \times E_2$ matrix was obtained as shown in Fig. 2 ; energy distribution shows that the most probable mass split is symmetrical.

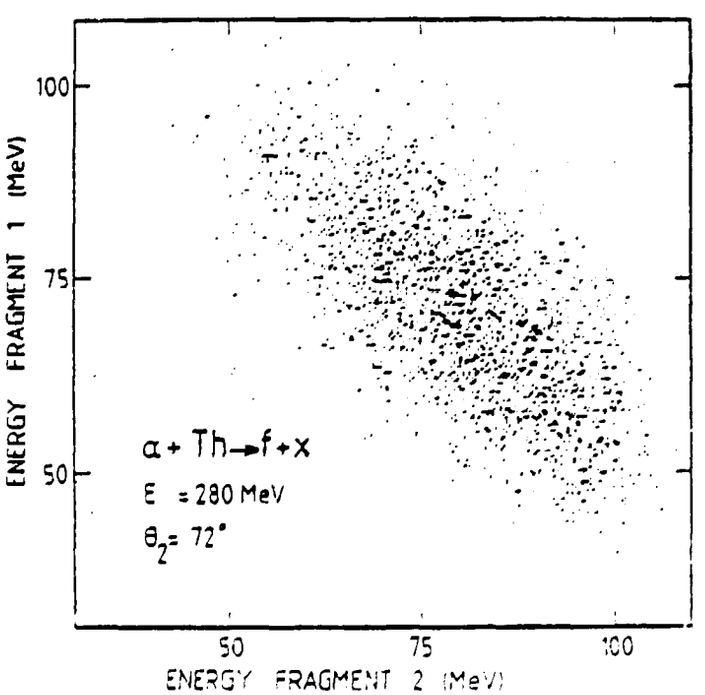

Fig. 2 - Energy distributions of the two fragment fission (E_1, E_2).

Contour diagrams of typical angular correlations between the two-fission fragments are shown in Fig. 3. Arrows at 180 indicate the location where the momentum transfer is zero. The ellipsoidal shapes come from

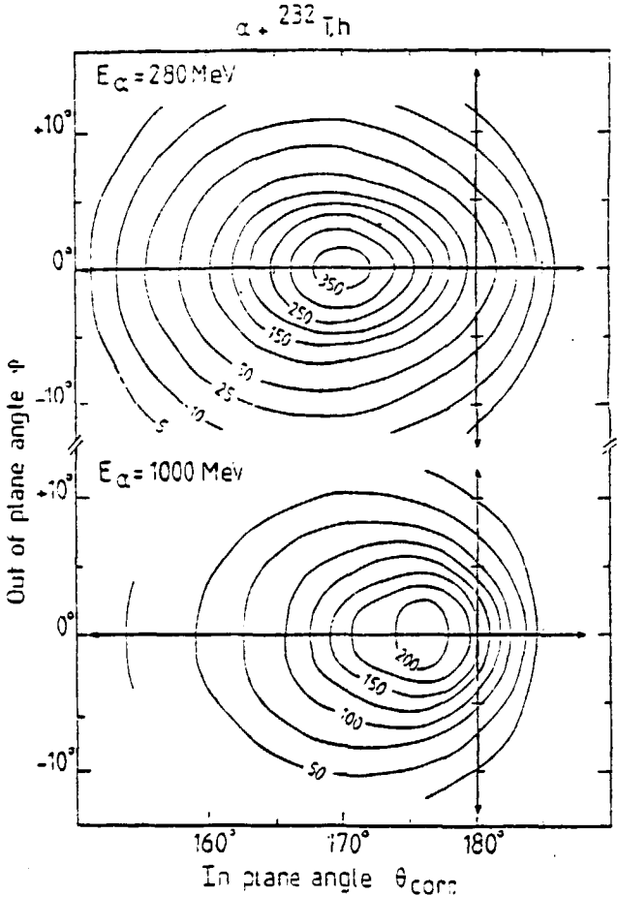

the momentum distribution from full transfer up to zero.

Fig. 3 - Two-dimensional correlation diagram of the fission fragments. Contour lines represent $d^2\sigma/d\Omega_1 d\Omega_2$ in arbitrary units. $\theta_{corr} = \theta_1 + \theta_2$.

In-plane angular correlations are presented in Fig. 4 at low energies the maximum is close to full momentum transfer (arrows) ; as the incident energy increases, the maximum of the angular correlations goes away from the full momentum transfer location, and the distribution become wider. For a given forward momentum $p_{//}$, an inherent dispersion of the correlation functions arises from many factors such as neutron emission of the fragments, distribution of masses, perpendicular component of the momentum, experimental angular resolution. The analysis achieved in order to extract the $p_{//}$ distributions is discussed in the next section.

III. Angular correlation between fission fragments

1. Momentum distributions. In these experiments, one considers the fission decay of the recoiling nucleus as an independent event in a chain of subsequent mechanisms. In fact one assumes fast processes ($\sim 10^{-22}$ sec) between projectile and target which produce many different reactions whose mechanisms are not well known. Then after emission of several fast particles, the residual nuclei are left with only a fraction of excitation energy, angular and linear momentum, the compound nucleus would have received. There exists a distribution of nuclei in different states which deexcite mainly by emitting nucleons and it is during this phase, considerably slower than the first stage of interaction, that fission occurs. One, therefore, does not know in detail the identity of the fissionning nucleus.

In order to extract, from the present data, the distribution of forward momenta, the angular correlations have been decomposed into 11 gaussian curves. This number was arbitrarily fixed and their angle locations correspond to 0., 0.1, 0.2 ... 1.0 time

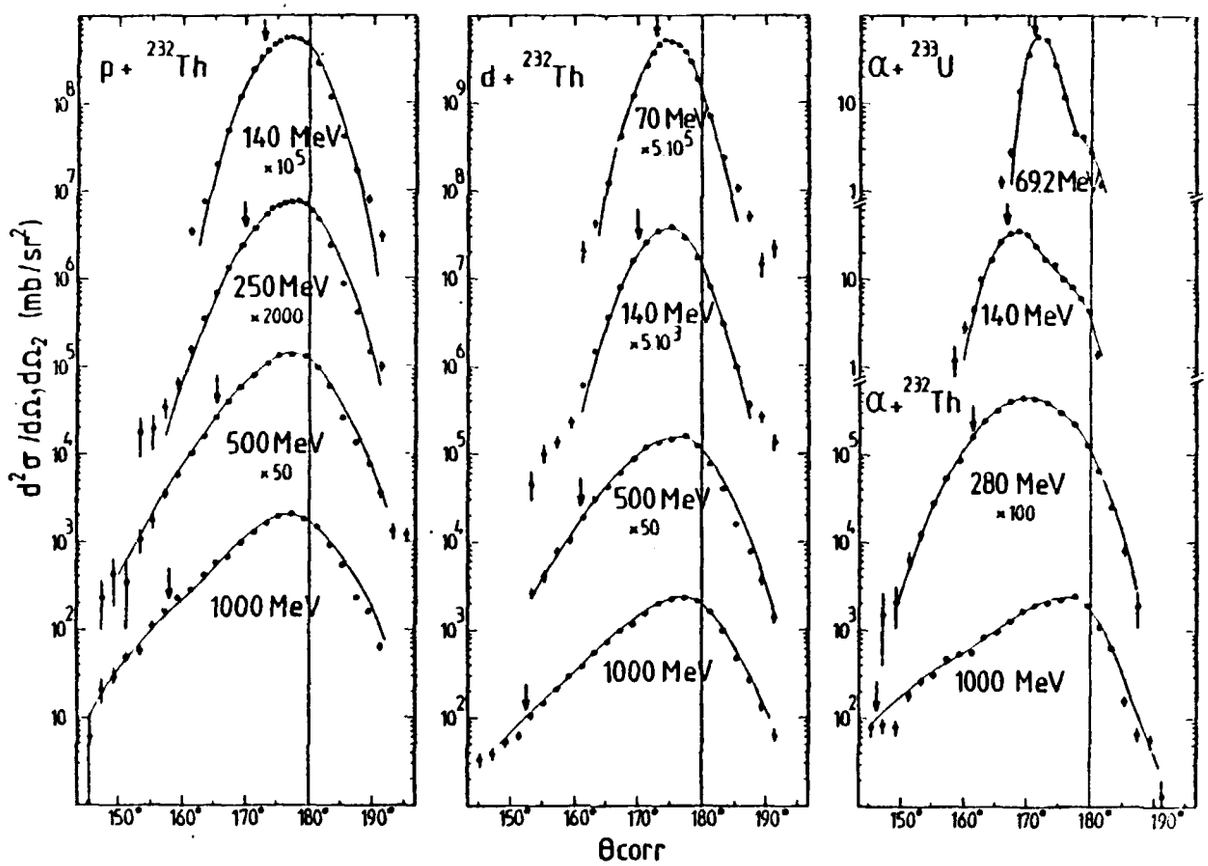

Fig. 4 - In-plane correlation function. Arrows indicate full momentum transfer. Solid lines are obtained by gaussian decomposition as explained in the text.

the full momentum transfer. Their widths are given by the out-of-plane measurements at the associated planar angles. An example of such unfolding procedure is presented in Fig. 5 ; the solid line is obtained by adjusting the relative weight of these gaussian curves in order to fit the experimental data. The derived momentum distributions are presented in Fig. 6. It should be noticed that these distributions cannot be uniquely determined from this method ; straightforward least square fits generate structures in the momentum distributions which are not justified. However reliable informations can be obtained for the shape and the gross behaviour of these distributions.

It is interesting to notice that the inelasticity ($p_{//}/p_{total}$) of these collision decreases regularly with the total incident energy and tends to the same value ($\simeq 0.15$) at 1 GeV incident for proton, deuteron and alpha particles. At high incident energies the momentum distributions are narrow because the out-plane width are considerably larger than at low energies and thus only few gaussian curves are necessary in the unfolding analysis.

Furthermore, up to 35 MeV/A, the full momentum transfer represents an important component (30-40) for the different interaction leading to fission as illustrated in

Fig. 7. But at 70 MeV/A, this contribution amounts for less than 5 % and become negligible at higher energies. These trends are similar for deuterons and alpha projectiles. If the full momentum transfer is associated with compound nucleus formation, then one has determined the transition region for such process at least for these kind of target nuclei.

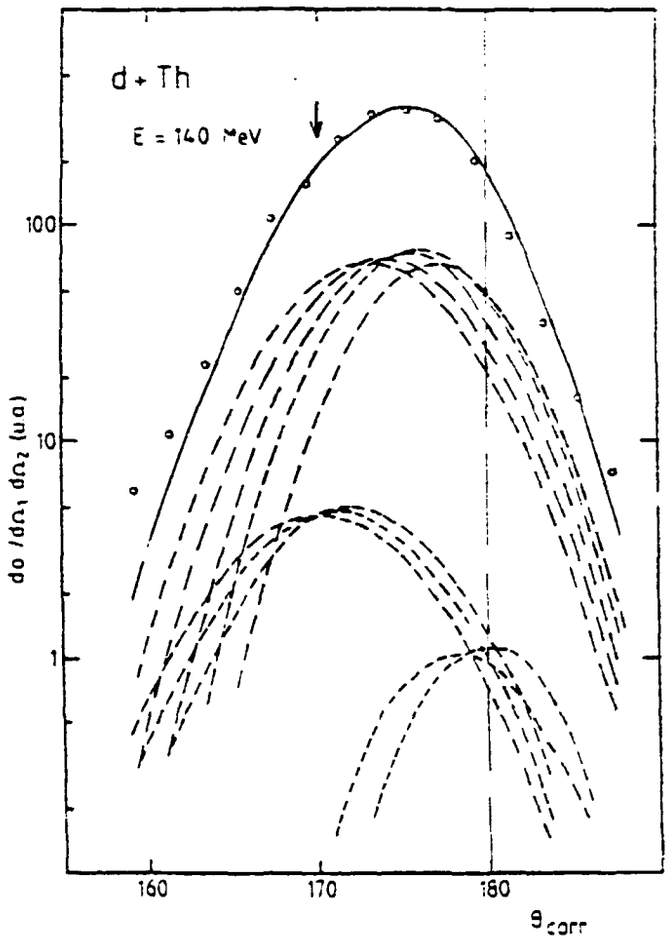

Fig. 5 - Gaussian decomposition obtained to fit the correlation function for d + ^{232}Th at 140 MeV.

We performed some intranuclear cascade calculation for the α + ^{232}Th at 1000 MeV, using the code (INC) developed by Yariv and Fraenkel [3]. In the first part of this two step calculation, the INC code (ISABEL) performs the nucleon-nucleon collisions leading to a residual nucleus distribution indicating their states (excitation energy, angular and linear momenta). Then, in a second part, a statistical theory code (EVA) selects those events leading to fission decay. The predicted momentum distribution is presented in Fig. 8 and compared to data. One notices that the overall agreement is fair, while the predicted momentum distribution is shifted towards smaller $p_{//}$ values than experimental values. The interest of such calculation is illustrated by the information given in Fig. 9. Residual nuclei decaying by fission have essentially less than 250 MeV excitation and 25$\hbar$ angular momentum, Fig. 9a,b. Those nuclei with higher excitation and spins decay by other processes, probably nucleon evaporation and total explosion. In this calculation, fissionning nuclei have A = 230 ± 6, while those which decay by other processes are lighter, Fig. 9c, probably because of their higher fission barrier. At last, the single nucleon-nucleon collision is the predominent mode compared to the other (sum of twofold and threefold collisions) for impact parameters ranging from 6 to 10 fermis and is probably overestimated since the predicted momentum distribution is too low compared to experiment, Fig. 8.

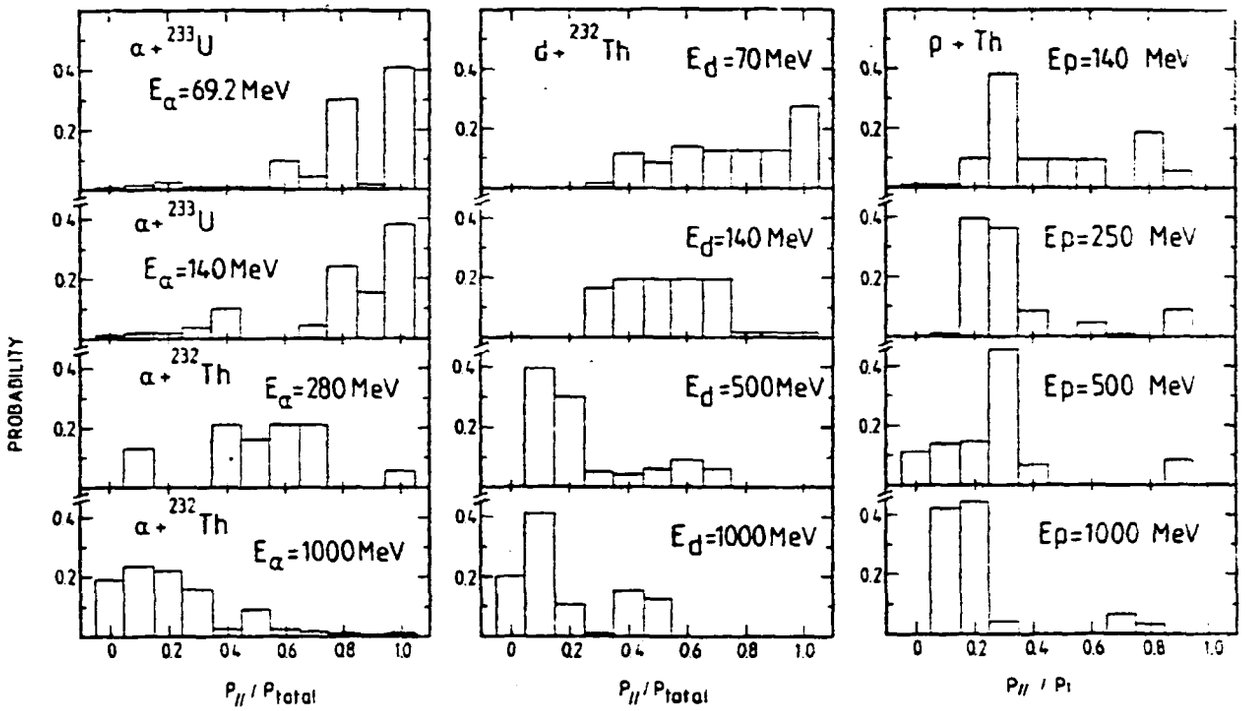

Fig. 6 - Probability distribution of the transferred linear momenta obtained by gaussian unfolding.

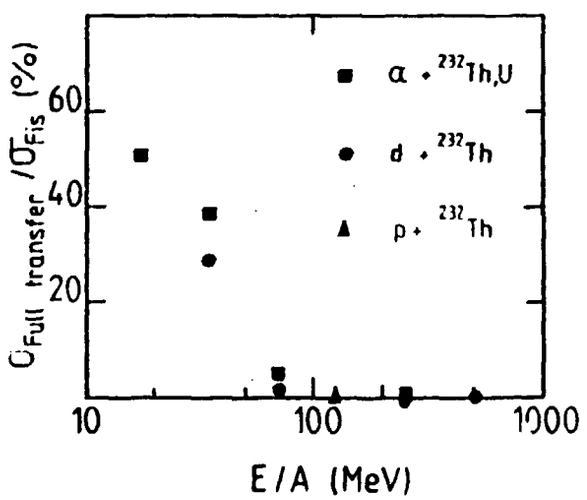

Fig. 7 - Ratio of the full transfer normalized to all transfer probabilities leading to fission versus the incident energy of projectiles. Data at 17.30 and 35 MeV alpha particles on U are from ref. [1].

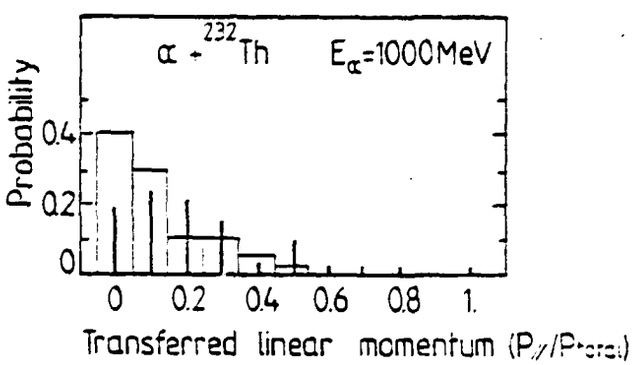

Fig. 8 - Comparison of probability distribution of transfer momentum (solid lines) with intra-nuclear cascade predictions (solid histogram).

2. Mean momentum transfer. An essential quantity which can be discussed is the average linear momentum transferred to the target ; this quantity divided by the mass number of the projectile is plotted in Fig. 10, versus the incident energy per nucleon. The solid line represents the full momentum transfer. This figure tests a "scaling", i.e. if an alpha particle transfers four times the momentum of a proton,

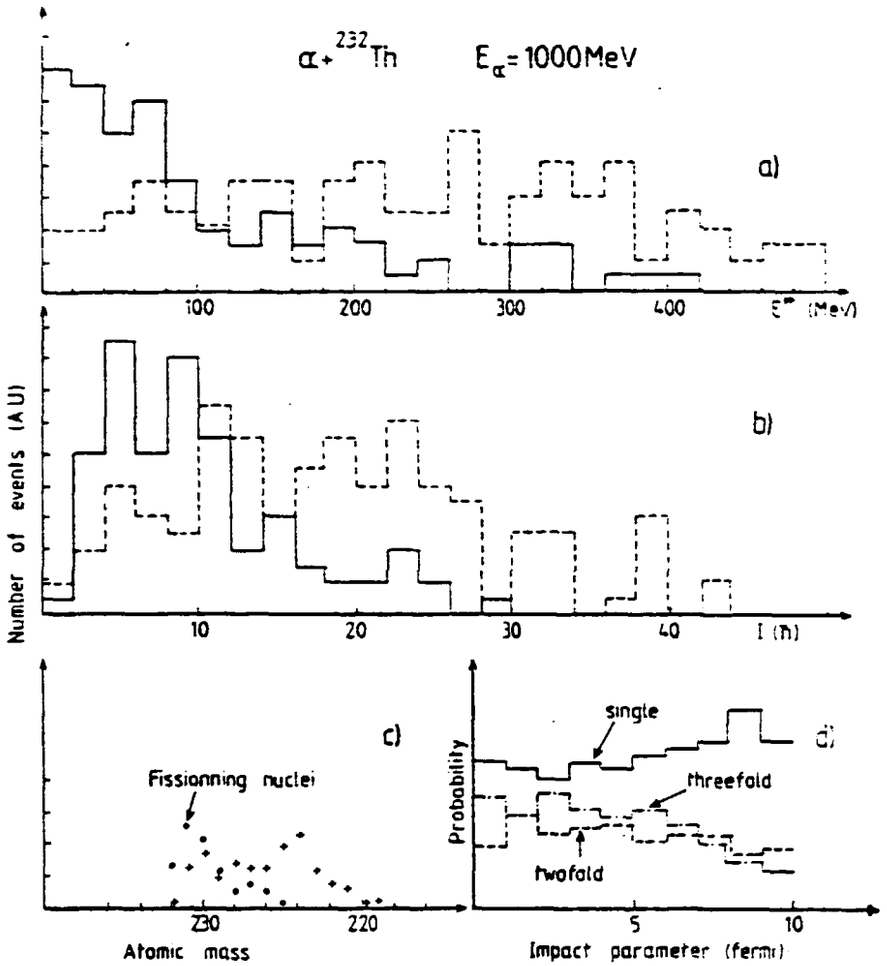

Fig. 9 - Intranuclear cascade predictions for α + ^{232}Th at 1000 MeV alpha particle incident energy. a) residual nucleus excitation energies-solid histogram is for fissionning nuclei and dashed one for no-fissionning nuclei. b) residual nucleus spin distribution. Histogram same as in a). c) residual nucleus mass distribution circles for fissionning nuclei ; crosses for no-fissionning nuclei. d) single, two-fold, three-fold collision probabilities versus impact parameter.

then the data points relative to alpha particles and protons will fall together. By this figure we attempt to classify the dominating reaction mechanisms in the various energy regimes : i) below 10 MeV/u, the incident particles transfer their momentum almost completely to the target. Complete fusion is the dominating process even for ^{16}O and ^{20}Ne projectiles ; ii) between 10 MeV/u and about 70 MeV/u, the data points fall below the full transfer curve but still more than half of the incident beam momentum is transferred to the target. Furthermore alpha particles and deuteron still exhibit a scaling, i.e., the transferred momentum is proportional to the mass of the projectile. This regime resembles the low energy behaviour with a contribution from preequilibrium processes ; iii) the 70 MeV/u to about 1000 MeV/u energy range corresponds to a transition region characterized by several features. The data points fall drastically below the full momentum transfer location. Furthermore while the momentum transferred by protons continues to increase with energy, those transferred by

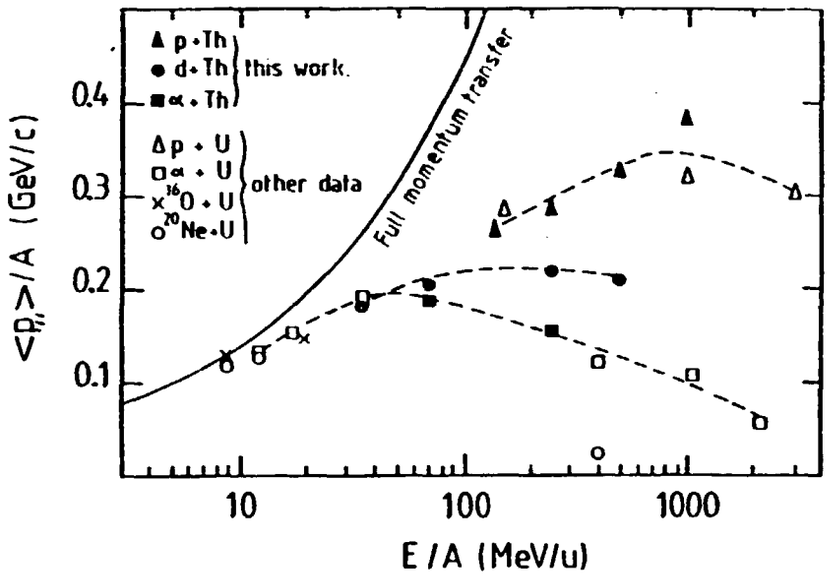

Fig. 10 - Mean momentum transfer per nucleon versus incident energy per nucleon. Solid line is for the full momentum transfer. Dashed lines are to guide eye. Open symbols and crosses are for other data : p + U refs. [9,10], α + U ref. [11], ^{16}O + U ref. [12], ^{20}Ne + U refs. [10,13].

deuterons and alpha particle drop with different slopes i.e., the scaling observed in ii) is lost. At 1000 MeV/u, alpha particles transfer as much *total linear momentum* as a proton of the same velocity, while 400 MeV/u ^{20}Ne projectiles behave like deuterons and alpha particles. This behavior is illustrated in Fig. 11, while shows the *total* transferred momentum versus the incident energy per nucleon. This observation

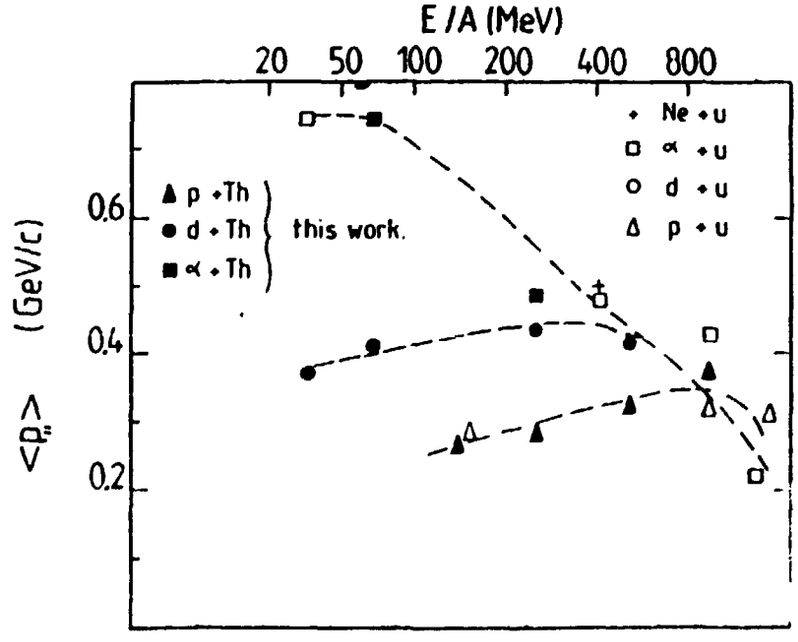

Fig. 11 - Same as Fig. 10 except that total $p_{\parallel}$ is plotted versus energy incident per nucleon. Data points have same references as in Fig. 10.

contredicts an interpretation in term of mechanisms dealing with central collisions since in this case, even nucleon-nucleon interaction should lead to momentum transfer dependent on the number of incident nucleons. Thus, reactions leading to fission decay are probably more peripheral and light particles are emitted in the earlier stages of the interaction (inelastic scattering, projectile breaks up, preequilibrium particles...). More violent collisions feed competiting channels leading to events out of the present experimental set-up oriented on fission decay.

III. Angular distributions of fission fragments

1. Differential cross section. The angular distributions of the single fission fragments have been measured from 10° up to 170° in order to obtain informations on the spins of the fissionning nuclei and to derive the total fission cross sections. They are presented in Fig. 12 in the laboratory system and show all forward peaking.

The angular distributions in the laboratory system have been converted in the center-of-mass system by varying the average velocity of the moving system in order to obtain a symmetric angular distribution around 90° (cm). The transformed points are plotted in Fig. 13 at the correspondingly transformed angles. This procedure yields an estimation of the average momentum transfers which is independent from the angular correlation measurements. Both values are compared in Table 1 ; they are both in good agreement proving that we observe undisturbed binary events. Another point of interest is that angular distribution shown in Fig. 13 exhibit rather flat pattern. Since the anisotropy, is governed by the nuclear temperature and the spin, roughly like J^2/T ; thus the higher the spin,the more the curve approaches a $1/\sin\theta$ distribution, the higher temperature,the flatter is the distribution. We performed calculation of the anisotropy using the relation [4]

$$W^{I}_{M=0}(\theta) = \frac{\pi/2(2J+1)\ \exp\left[-(J+1/2)^2\ \sin^2\theta/4K_0^2\right]\ J_0\left[i(J+1/2)^2\ \sin^2\theta/4K_0^2\right]}{2\pi(\pi^{1/2}/2)\ (2K_0^2)^{1/2}\ \mathrm{erf}\left[(J+1/2)\ /\ (2K_0^2)^{1/2}\right]}$$

J_0 is the zero order Bessel function and erf(J+1/2) is the error function. The value K_0^2 depends on the moment of inertia and on the temperature ; and J is the average spin of the fissionning nuclei. As we are dealing with small anisotropies, the dependence on the temperature contributes weakly ; so we assumed for the analysis the higher possible excitation energies. Then the spin values extracted in this way are upper limits ; they are listed in Table 1 and compared to grazing angular momenta. Above 100 MeV/n incident energies, spins values are less than 10ħ ; these small values might be due in part to inelastic process which transfer small amount of angular momentum, and in other part to neutron evaporation before fission which carry away few ħ and contribute to disoriente the influence of J on the observed anisotropy.

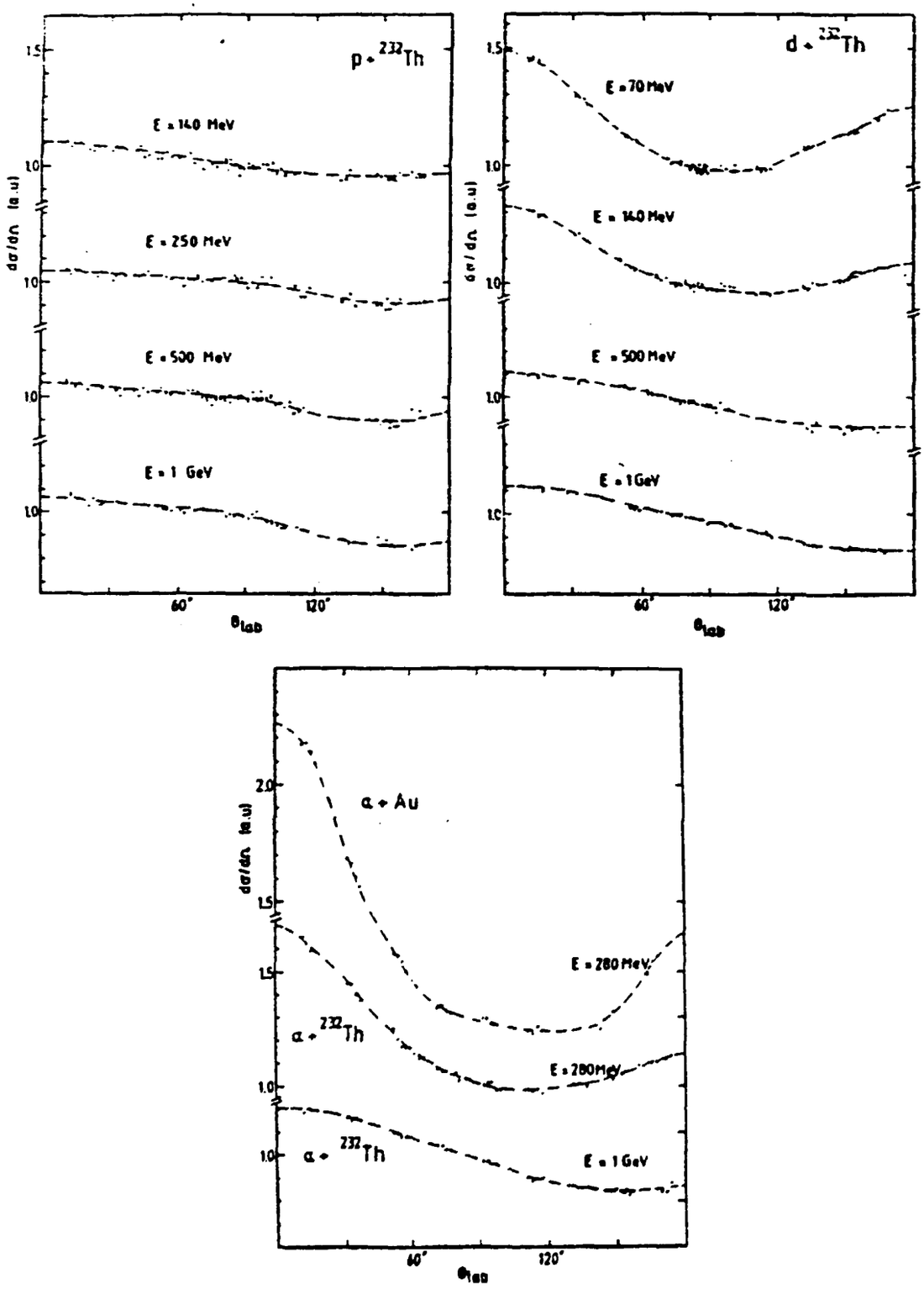

Fig. 12 - Angular distributions of fission fragments (singles) ; dσ/dΩ are in arbitrary units and in the laboratory system. Lines are to guide eyes.

INC calculations predicts in average such low angular momentum of fissionning nuclei as shown in Fig. 9. In fact, events with J values higher than 10ħ seem to arise from central collisions, to correspond to high excitation energies and to decay by another channels than fission.

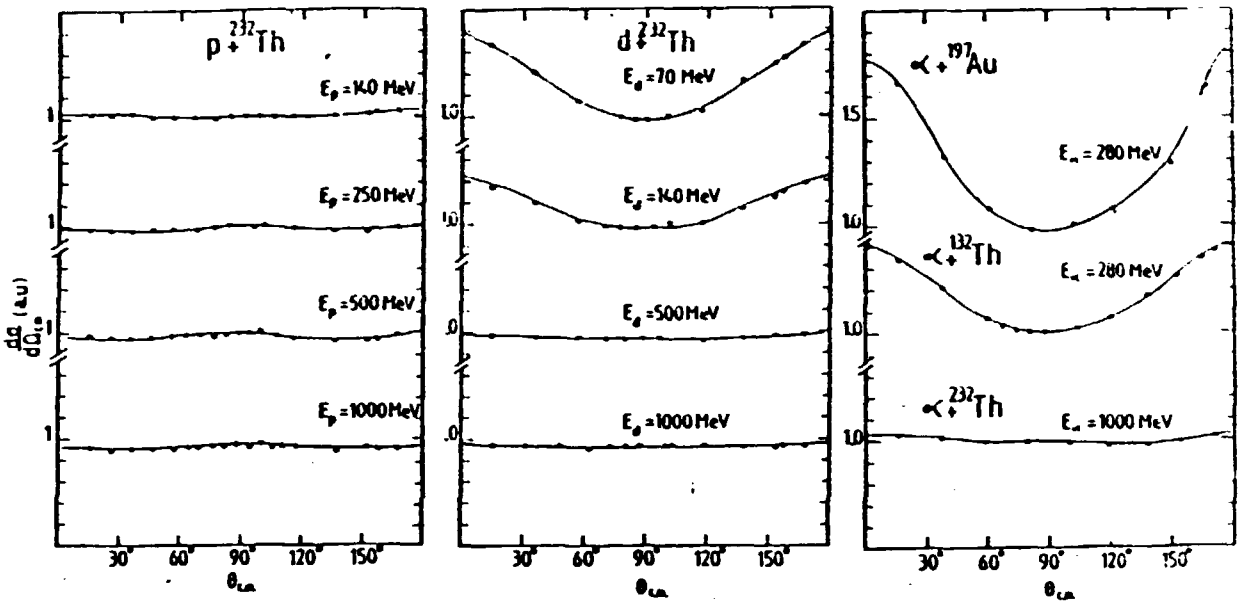

Fig. 13 - Angular distributions of fission fragments (singles) transformed in the system of the fissionning nuclei.

Table 1

Systems	E_i (MeV)	$\bar{p}_{//}$(AD) (MeV/c)	$\bar{p}_{//}$(AC) (MeV/c)	ℓ_{gr} (ħ)	J_{fiss} (ħ)	σ^{exp}_{fiss} (mb)
p + ^{232}Th	140	307 ± 25	263	25	4	1210 ± 120
"	250	314 ± 25	281	34	1	1130 ± 115
"	500	310 ± 25	308	49	1	1210 ± 120
3	1000	490 ± 50	385	70	1	1200 ± 120
d + ^{232}Th	70	377 ± 30	375	25	13	1640 ± 160
"	140	456 ± 40	417	37	11	1600 ± 160
"	500	532 ± 40	437	72	5	1320 ± 130
"	1000	620 ± 60	430	102	4	1350 ± 135
α + ^{232}Th	280	867 ± 80	757	75	17	1960 ± 190
"	1000	754 ± 80	611	148	7	1520 ± 150

$\bar{p}_{//}$(AD) are derived from fission fragment angular correlations. $\bar{p}$ (AC) are derived from in-plane angular correlations. Errors are of the order of ± 35 MeV/c.

2. Integrated fission cross section. Fission cross sections are obtained by integrating angular distributions. Absolute values are plotted in Table 1 as well as experimental errors estimated to ± 10 % due to target thickness and integrated beam uncertainties. Fission excitation functions are presented in Fig. 14. The trends for proton and deuteron are rather flat ; in contrary the slope for alpha data is steeper. Reaction cross section have been estimated using different results found in the litterature (dashed curves in Fig. 14). Renberg et al. [5] achieved systematic analysis of reactions cross section (σ_R) in a wide range of proton energies and target nuclei. They estimate σ_R around 1800 mb for the p + ^{232}Th at 560 MeV. They also analyzed reaction cross section on lead target from 70 to 600 MeV. We used their results for the ^{232}Th target by adjusting radius differences (7). Theoretical reactions cross section for

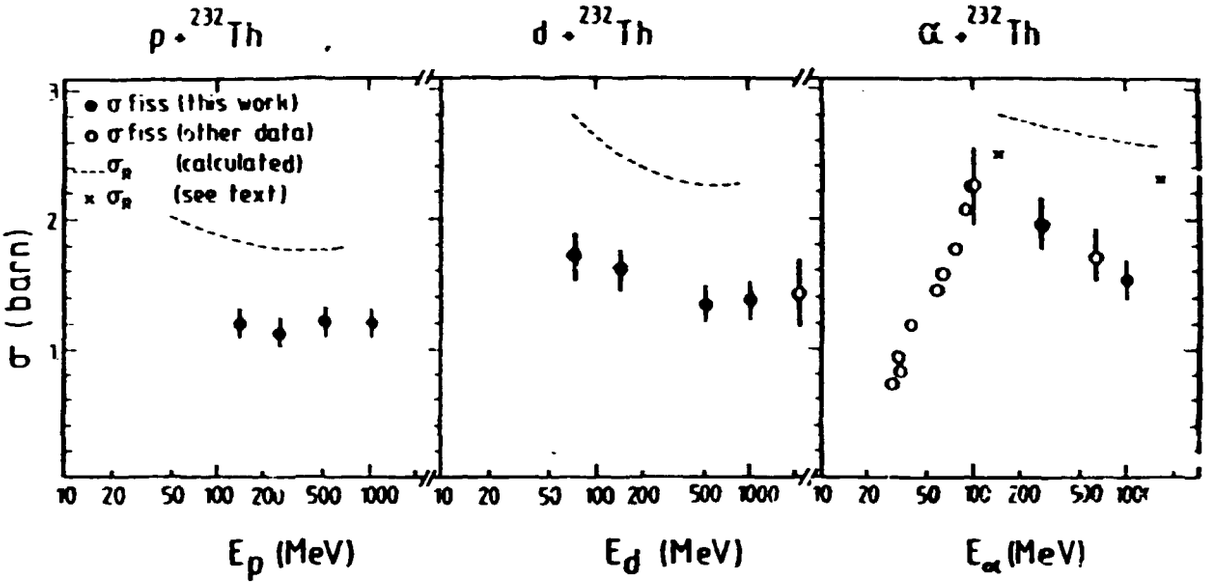

Fig. 14 - Integrated fission cross sections versus incident energies. The value at 2.1 GeV deuteron is from ref. [10]. Other data for α induced fission are from ref. [1]. Dashed line are reaction cross section calculations from ref. [5] for proton, from ref. [6] for deuteron and alpha particles. The cross at 140 MeV alpha is an experimental reaction cross section from ref. [1] and at 1.6 GeV is a theoretical one from refs. [7,11]

deuteron and alpha projectiles are from DeVries calculations [6] on lead target ; by adjusting the size corrections we deduced σ_R for the thorium target as shown in Fig. 14. At 140 MeV alpha particle [1], the experimental cross section is indicated by a cross showing that the theoretical σ_R [6] are overestimated. The cross at 1600 MeV is a theoretical value from another calculation [7,11]. These two last values seem to show that theoretical σ_R performed by DeVries [6] might be overestimated in the whole energy range.

The striking feature of the comparison illustrated in Fig. 14 is that $\sigma_{fiss}/\sigma_R \simeq 2/3$ in the wide range of incident energy ; this means that the more violent collisions exhaust at all these energies about 1/3 of the σ_R. Apparently whatever happen in the first stage, one ends up always at the same division between fission and other processes.

REFERENCES

[1] W.G. Meyer, V.E. Viola Jr., R.G. Clark and S.M. Read, Phys. Rev. C20 (1979) 116.

[2] T. Sikkeland, E.L. Haines and V.E. Viola Jr., Phys. Rev. 125 (1962) 1350.

[3] Y. Yariv and Z. Fraenkel, Phys. Rev. C20 (1979) 2227. The INC code was made kindly available for us by Dr. Blachot (CEN Grenoble).

[4] R. Vandenbosch and J. Huizenga, Nuclear fission (Academic, New York, 1973).

[5] P.U. Renberg et al., Nucl. Phys. A183 (1972) 81.

[6]

[7] P.J. Karol, Phys. Rev. C11 (1975) 1203.

[8] A.A. Kotov, G.G. Semenchuck, B.A. Bochagov, B.L. Gorshkov, G.G. Kovshevnyĭ, V.R. Reznik and G.E. Solyakin, Sov. J. Nucl. Phys. 17 (1973) 498.

[9] C.J. Stephan and L.M. Perlman, Phys. Rev. 164 (1967) 1528.

[10] L.P. Remsberg, F. Plasil, J.B. Cumming and M.L. Perlman, Phys. Rev. 187 (1969) 1597.

[11] W.G. Meyer, H.H. Gutbrod, Ch. Lukner and A. Sandoval, Phys. Rev. C22 (1980) 179.

[12] B.B. Back, K.L. Wolf, A.C. Mignerey, C.K. Gelbke, T.C. Awes, H. Breuer, V.E. Viola Jr and P. Dyer, Phys. Rev. C22 (1980) 1927.

[13] V.E. Viola Jr., R.G. Clark, W.G. Meyer, A.M. Zebelman and R.G. Sextro, Nucl. Phys. A261 (1976) 174.

[14] L.P. Remsberg, F. Plasil, J.B. Cumming and M.L. Perlman, Phys. Rev. 187 (1969) 1597.